Nanoparticles

How to cite:
International Edition: doi.org/10.1002/anie.202008018
German Edition: doi.org/10.1002/ange.202008018

J-Aggregate-Based FRET Monitoring of Drug Release from Polymer Nanoparticles with High Drug Loading

*Yun Liu[+], Guangze Yang[+], Song Jin, Run Zhang, Peng Chen, Tengjisi, Lianzhou Wang, Dong Chen, David A. Weitz, and Chun-Xia Zhao**

Abstract: *Understanding drug-release kinetics is critical for the development of drug-loaded nanoparticles. We developed a J-aggregate-based Förster-resonance energy-transfer (FRET) method to investigate the release of novel high-drug-loading (50 wt %) nanoparticles in comparison with low-drug-loading (0.5 wt %) nanoparticles. Single-dye-loaded nanoparticles form J-aggregates because of the high dye-loading (50 wt %), resulting in a large red-shift (≈110 nm) in the fluorescence spectrum. Dual-dye-loaded nanoparticles with high dye-loading using FRET pairs exhibited not only FRET but also a J-aggregate red-shift (116 nm). Using this J-aggregate-based FRET method, dye-core–polymer-shell nanoparticles showed two release processes intracellularly: the dissolution of the dye aggregates into dye molecules and the release of the dye molecules from the polymer shell. Also, the high-dye-loading nanoparticles (50 wt %) exhibited a slow release kinetics in serum and relatively quick release in cells, demonstrating their great potential in drug delivery.*

Introduction

Polymer nanoparticles have attracted significant interest in drug delivery due to their excellent biocompatibility, biodegradability, and simple fabrication methods.[1] The FDA-approved biodegradable poly(D, L-lactic-co-glycolic acid) (PLGA) is a promising candidate for making polymer nanoparticles.[2] However, two main challenges remain for their clinical applications, that is, low drug loading (usually below 10 wt %) and undesirable burst release of the encapsulated drugs.[3] Drug loading here is defined as the mass fraction of the drug in the entire drug-loaded nanoparticles (w/w).[4] We reported previously a simple and robust sequential nanoprecipitation technology to produce stable drug-core polymer-shell nanoparticles with high drug loading (up to 58.5 wt %) from a wide range of polymers and drugs, providing a new opportunity to address these two challenges.[5] However, the drug release kinetics of these high drug-loading polymeric nanoparticles remain unexplored.

Förster resonance energy transfer (FRET) has been widely used for investigating drug release kinetics.[6] It involves the energy transfer from one fluorophore to the other, shifting the fluorescence emission. FRET can be used to monitor the integrity and disassembly of fluorescent dye-loaded nanoparticles thus providing valuable spatial and kinetic information.[7] A hydrophobic FRET pair, 3, 3′-dioctadecyloxacarbocyanine perchlorate (DiO) as the donor and 1,1′-dioctadecyl-3,3,3′,3′-tetramethylindocarbocyanine perchlorate (DiI) as the acceptor, can be loaded into polymeric nanoparticles using nanoprecipitation.[8] The proximity (usually less than 10 nm) between the two dyes can induce the FRET effect.[9] When both DiO and DiI are encapsulated inside one nanoparticle, excitation of DiO would result in DiI emission. Then when the nanoparticle disassembles, recovery of the DiO emission could be observed due to the elimination of the energy transfer.[10] This strategy allows us to directly monitor the release of DiO and DiI from nanoparticles under different conditions.[6a]

Discovered more than 80 years ago by Jelley and Scheibe,[11] J-aggregates are formed by a highly ordered assembly of organic dyes with the spectroscopic properties significantly different from that of single or disorderly assembled dye molecules.[12] The key features of J-aggregates are the strong shift of their absorption and emission spectra to longer wavelengths with respect to the spectra of monomers together with their dramatic sharpening. In contrast, aggregates with absorption bands shifted to shorter wavelengths with respect to the monomer band are called H-aggregates.[13] J- and H-aggregates consist of stacked dye molecules in the head-to-tail arrangement (J aggregates) and a sandwich-type arrangement (H aggregates).[12]

To simulate drug-loaded nanoparticles, we used hydrophobic dyes as the model hydrophobic drugs. We synthesized dye-loaded polymeric nanoparticles (DiO, DiI and the DiO-DiI pair (FRET) ($W_{DiO}/W_{DiI}=1:1$)) with low dye loading

[*] Y. Liu,[+] G. Yang,[+] S. Jin, R. Zhang, Tengjisi, C.-X. Zhao
Australian Institute for Bioengineering and Nanotechnology, University of Queensland
St. Lucia, Queensland 4072 (Australia)
E-mail: z.chunxia@uq.edu.au
P. Chen, L. Wang
Nanomaterials Centre, School of Chemical Engineering, Australian Institute for Bioengineering and Nanotechnology, The University of Queensland
Brisbane, QLD, 4072 (Australia)
D. Chen
Institute of Process Equipment, College of Energy Engineering, Zhejiang University
Hangzhou, Zhejiang 310027 (China)
D. A. Weitz
John A. Paulson School of Engineering and Applied Sciences, Harvard University
Cambridge, MA 02138 (USA)
[+] These authors contributed equally to this work.
Supporting information and the ORCID identification number(s) for the author(s) of this article can be found under: https://doi.org/10.1002/anie.202008018.

(0.5 wt%; $W_{dye}/W_{dye+polymer}$) using the traditional bulk nanoprecipitation method and high dye loading nanoparticles (50 wt%) using our sequential nanoprecipitation method, to monitor and compare their release kinetics. A large red-shift (≈100 nm) was observed in the fluorescence spectra of DiO, DiI, and FRET-loaded nanoparticles with high dye loading due to the formation of J-aggregates. Based on this finding, we developed a new J-aggregate-based FRET approach to investigate the release kinetics of the high dye-loading nanoparticles. Furthermore, we compared the release and disassembly of low and high dye-loading nanoparticles in cells and serum using the traditional FRET method and our new J-aggregate-based FRET approach. Interestingly, we found that the high dye-loading nanoparticles had a unique release and disassembly kinetics, and their release was slower than that of the low dye-loading nanoparticles. To the best of our knowledge, this is the first J-aggregate-based FRET method to study the release kinetics of drug-loaded nanoparticles.

Results and Discussion

In our previous work, we reported a new sequential nanoprecipitation approach to fabricate polymer nanoparticles with exceptionally high drug loading using a wide range of drugs and polymers.[5,14] The sequential nanoprecipitation approach is based on tuning the precipitation time of drugs and polymers using a multi-solvent system, leading to the formation of drug nanoparticles followed by the instant precipitation of a polymer thus forming drug-core polymer-shell nanoparticles. Typically, a drug and a polymer at a 1:1 weight ratio are first dissolved in a solvent mixture of dimethyl sulfoxide (DMSO), dimethylformamide and ethanol. Phosphate buffered saline buffer at pH 7.4 is poured into this solution with gentle mixing (Figure 1), forming drug-core polymer-shell nanoparticles. In the case of using poly (D, L-lactide-co-glycolide)-block-poly(ethylene glycol) ($PLGA_{10K}$-PEG_{5K}) as the polymer and curcumin as the drug, curcumin-loaded polymeric nanoparticles with 58.5 wt% drug loading exhibit a multiple drug-core structure (Figure 1a4). This unique core–shell structure raises two questions: (1) How do the high drug-loading nanoparticles release the encapsulated drug? (2) Do they have similar intracellular release kinetics as those traditional nanoparticles having low drug loading?

To answer these questions, we developed a J-aggregate-based FRET method to investigate the structures and disassembly kinetics of high drug-loading polymeric nanoparticles, in comparison with the traditional low drug-loading nanoparticles. Fluorescent dyes DiO and DiI were selected for encapsulation because they are an efficient FRET pair with Förster distance of ca. 4 nm.[7b] Additionally, as hydrophobic dyes, they can be encapsulated in the polymeric nanoparticles in the same way as those hydrophobic drugs, thus mimicking the disassembly and release of drugs.

We synthesized $PLGA_{10K}$-PEG_{5K} nanoparticles with low dye loading (0.5 wt%; $W_{dye}/W_{dye+polymer}$) including DiO-loaded (Low-DiO), DiI-loaded (Low-DiI), and the DiO-DiI pair (FRET)-loaded nanoparticles (weight ratio $W_{DiO}/W_{DiI}=1:1$; Low-FRET) using the traditional bulk nanoprecipitation method (Figure 1b). We also synthesized dye-loaded $PLGA_{10K}$-PEG_{5K} nanoparticles with high dye loading (50 wt%; $W_{dye}/W_{dye+polymer}$) including DiO (High-DiO), DiI (High-DiI) and DiO-DiI pair ($W_{DiO}/W_{DiI}=1:1$; High-FRET) using our sequential nanoprecipitation method (Figure 1c), the encapsulation efficiencies of high dye loading nanoparticles fabricated using this method were more than 95%.[5] The TEM images show that the Low-DiO, Low-DiI and Low-FRET nanoparticles have similar structures as the plain $PLGA_{10K}$-PEG_{5K} nanoparticles, as the dye loaded inside the nanoparticles are mostly in molecular state which are too small to be observed under TEM (Figure 1d and Figure S1). In contrast, the High-DiO, High-DiI, and High-FRET nanoparticles contain several dye-cores of 30–40 nm (Figure 1e), similar to those high drug-loading $PLGA_{10K}$-PEG_{5K} nanoparticles.[5]

The FRET polymer nanoparticles (Low-FRET and High-FRET) showed much higher FRET ratios (FRET emission/donor emission) than that of the nanoparticle mixture (a mixture of Low-DiO and Low-DiI: Low-Mixture, or a mixture of High-DiO and High DiI nanoparticles: High-Mixture), indicating the successful co-loading of DiO and DiI in the FRET nanoparticles (Figures S2–7). To further confirm whether they contain individual DiO and DiI core nanoparticles, or hybrid DiO-DiI core nanoparticles, we precipitated DiO, DiI and the DiO-DiI pair ($W_{DiO}/W_{DiI}=1:1$) into nanoparticles without polymer to mimic the formation of dye cores as the plain dye particles can be stable for 1–3 hours. To precipitate DiO and DiI, two types of nanoparticles might form: hybrid FRET nanoparticles incorporating both DiO and DiI in a single particle, or a mixture of individual DiO and DiI nanoparticles. For hybrid FRET nanoparticles, we should be able to observe a strong FRET emission. Otherwise, there should be no FRET emission and the suspension should have a similar spectrum as the mixture of DiO and DiI nanoparticles ($W_{DiO}/W_{DiI}=1:1$) due to the long distance between the DiO and DiI nanoparticles and their self-quenching effect. In the experiments, the hybrid FRET nanoparticles showed a strong FRET peak with similar spectra and fluorescence photo as the High-FRET polymer nanoparticles (Figures S8–11), confirming that the DiO and DiI are co-precipitated as hybrid FRET cores, which is ideal for investigating the release kinetics of the High-FRET nanoparticles. All the nanoparticles including the Low-DiO, Low-DiI, Low-FRET, High-DiO, High-DiI, High-FRET, DiO nanoparticles, DiI nanoparticles, and hybrid FRET nanoparticles, have hydrodynamic sizes in the range of 82–139 nm (Figure 1 f,g, Figure S12, 13 and Table S1). The nanosuspensions of Low-DiO, Low-DiI, and Low-FRET nanoparticles are clear solutions without any aggregates and had similar colors (yellow, pink and red colors, respectively) as those samples of High-DiO, High-DiI, and High-FRET under bright-field observation (Figure 1h,i).

Figures 2a–c show the fluorescence spectra and images of the low and high dye-loading polymeric nanoparticle suspensions containing the donor dye DiO, acceptor dye DiI, or the FRET pair DiO-DiI. To compare the changes of spectra in the following experiments, we divided the wavelength from

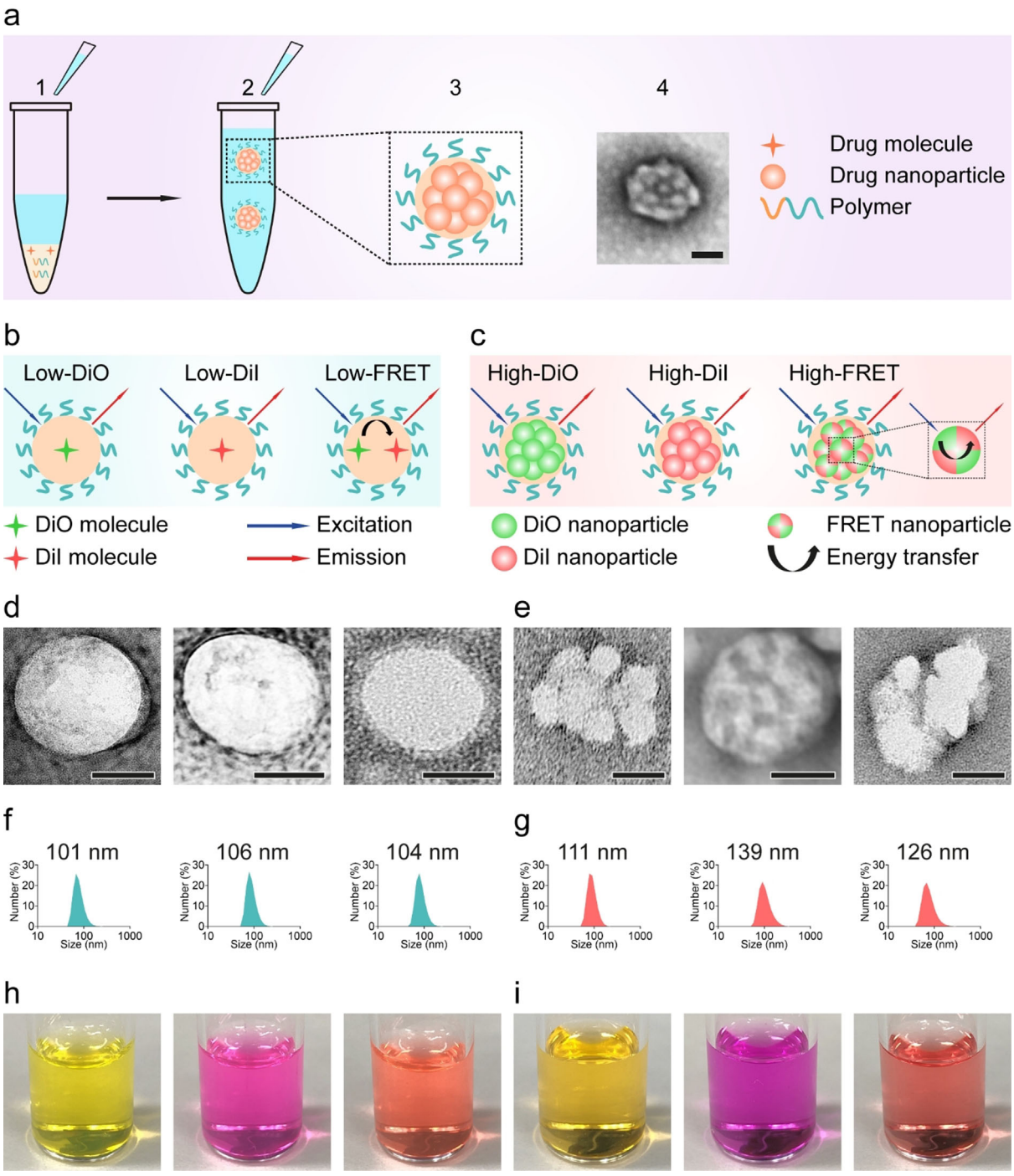

Figure 1. Synthesis and characterization of dye-loaded polymeric nanoparticles (DiO, DiI and FRET pair) with low and high dye loading. a) Our sequential nanoprecipitation approach. An anti-solvent is added to a three-solvent mixture containing a hydrophobic drug and a polymer under gentle mixing (1). Uniform drug nanoparticles precipitate first and form clusters, followed by the precipitation of polymer covering the drug nanoparticle cluster (2), thus forming a drug-core polymer-shell structure (3). The TEM image shows a core–shell structure with several drug nanoparticles in the core (4). The schemes (b and c), TEM images (d and e), DLS results in number % (f and g) and photos of suspension (h and i) of the low dye-loading (0.5 wt%) polymeric nanoparticles: Low-DiO, Low-DiI, and Low-FRET nanoparticles (b, d, f and h from left to right) and high dye-loading (50 wt%) polymeric nanoparticles: High-DiO, High-DiI, and High-FRET nanoparticles (c, e, g and i from left to right). The scale bars for d and e are 50 nm.

450 nm to 750 nm into three areas based on the peaks of DiO and DiI molecules or nanoparticles: (I) 450–550 nm (green), (II) 550–650 nm (orange) and (III) 650–750 nm (red). The Low-DiO and High-DiO nanoparticles showed very different fluorescence spectra mainly due to the formation of DiO J-aggregates in the High-DiO nanoparticles (Figure S14). Moreover, the maximum emission of High-DiO showed a dramatic red shift (112 nm) from 507 nm to 619 nm, leading

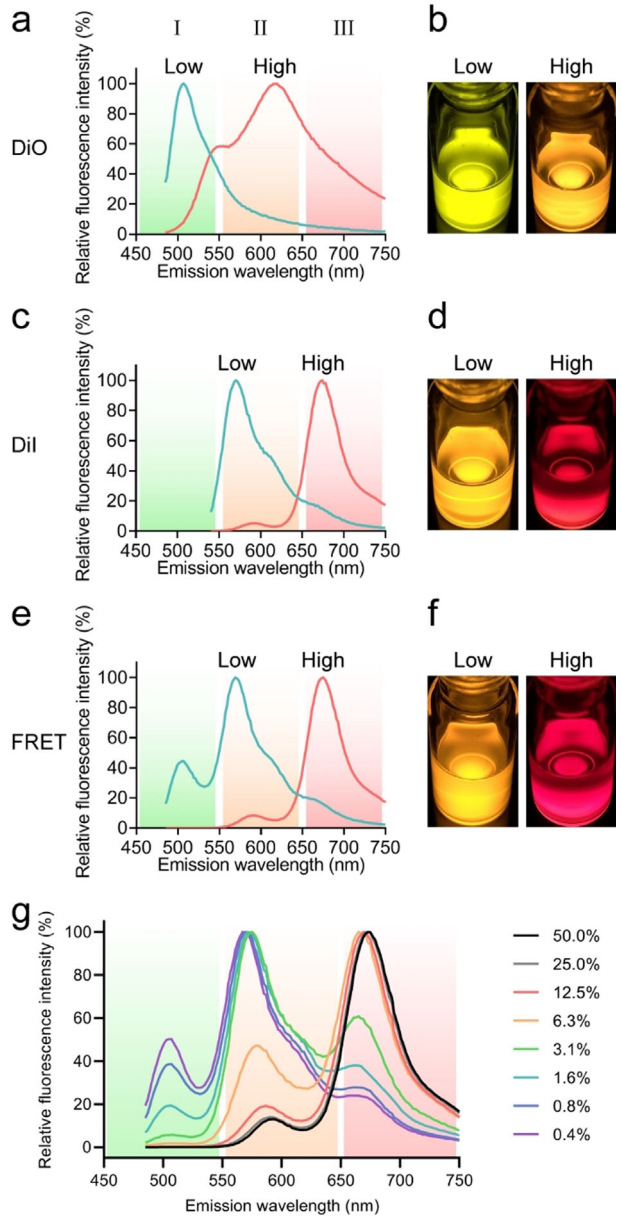

Figure 2. Spectra and fluorescent photos of the low and high dye-loading nanoparticles loaded with DiO (a,b), DiI (c,d), J-aggregate-based FRET with a big red-shift (e,f) and the spectra of FRET dye loaded nanoparticles from 0.4 wt% dye-loading to 50 wt% (g). The wavelength of spectra is divided into 3 areas, (I) 450–550 nm marked with green color, (II) 550–650 nm marked with orange color and (III) 650–750 nm marked with red color.

to different fluorescence colors of the Low-DiO and High-DiO, that is, green and orange, respectively (Figure 2a,b). This is consistent with other dyes as similar red shifts were observed previously for Cy3 and Cy7.5 dyes with an increase in the dye content.[15] Similarly, we also observed a large red shift (104 nm) of the Low-DiI and the High-DiI spectra from 570 to 674 nm and a fluorescence color change from orange-yellow to red (Figure 2c,d).

FRET technology has been widely used to monitor the release and disassembly of polymeric nanoparticles with relatively low drug loading. Consistent with what others found,[6c,f,16] we also observed the FRET peak of the Low-FRET nanoparticles which was similar to the peak of the acceptor dye-loaded nanoparticles (Low-DiI). In contrast, the High-FRET nanoparticles showed a red-shift FRET peak (106 nm) compared to the FRET peak of the Low-FRET nanoparticles (Figure 2e). This was expected, as we demonstrated above that the High-FRET nanoparticles had hybrid FRET cores as a result of the co-precipitation of DiI and DiO forming J aggregates. Consequently, the Low-FRET (orange-yellow) and High-FRET (red) showed similar colors as those of the Low-DiI and High-DiI nanoparticles (Figure 2f).

To further demonstrate this unique J-aggregate-based FRET phenomenon, we prepared FRET nanoparticles with different dye loadings from 0.4, 0.8, 1.6, 3.1, 6.3, 12.5, 25 and 50 wt% (Figure 2g). We can see that when the dye loading was lower than 3.1 wt%, a normal FRET peak was observed. The FRET ratio II/I (fluorescence intensity of peak at area II/ peak at area I) increased from 1.99 to 17.27, and the FRET ratio III/II (fluorescence intensity of peak at area III/ peak at area II) increased from 0.24 to 0.61 with the increase of dye loading from 0.4% to 3.1% (Table S2). However, for dye loading higher than 3.1 wt%, the J-aggregate based FRET shift was significant. The FRET ratio III/II increased from 0.61 to 9.7 along with the increase of dye loading from 3.1% to 50% (Table S2). The self-quenching of the acceptor dye occurred above 6.3% of dye-loading, as evidenced by the decrease of the intensity of FRET peaks at area III (Figure S15). This demonstrates the direct correlation between the red shift of the FRET peak and dye content in the nanoparticles, allowing us to use the J-aggregate FRET phenomenon to monitor the release kinetics of our high dye-loading nanoparticles. The formation of J-aggregate is common as organic dyes tend to π-stack into aggregates. Different approaches have been developed to prevent dye aggregation and dye self-quenching, for example, by using bulky hydrophobic counterions as spacer.[17]

To mimic the swelling and disintegration processes of the low and high drug-loading nanoparticles, we used an accelerated method by adding excess water-miscible organic solvent DMSO until a final DMSO of 95%, to destroy the core–shell structure completely by dissolving both the polymer and the dye. The spectra and fluorescent colors of the Low-DiO and Low-DiI nanoparticles were similar at both 0% and 95% DMSO, implying that the dye loaded in the low dye-loading nanoparticles was in molecular states (Figure 3a,b and Figure S16). For the Low-FRET nanoparticles, the spectrum peaked at area at 0% DMSO, then the peak moved to the area after adding 95% DMSO with a strong emission of the donor dye but a complete disappearance of the emission from the acceptor dye (Figure 3a,b and Figure S16) with the FRET ratio II/I decreased from 2.25 to 0.21 (Table S3). This is consistent with others' work[9,13,16] and confirmed the good integrity of the Low-FRET nanoparticles without DMSO, wherein DiO and DiI molecules were in very close proximity within the nanoparticles. So the integrity of particles can be assessed based on the FRET signal. In contrast to the low drug-loading nanoparticles, both the High-DiO and High-DiI nanoparticles had a big peak shift after

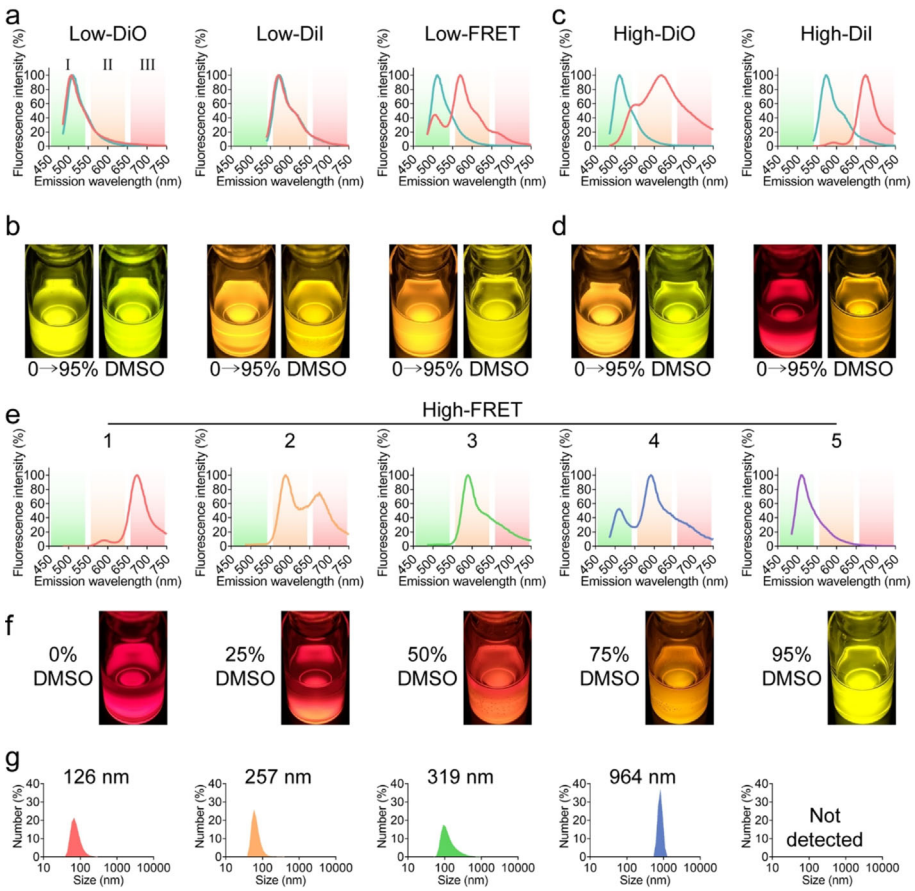

Figure 3. The disintegration of the low and high dye-loading nanoparticles using an accelerated dissolving process in DMSO from 0% to 95% (volume ratio). The spectra and fluorescence photos of the low dye-loading nanoparticles: Low-DiO, Low-DiI, Low-FRET (a,b) and high dye-loading nanoparticles: High-DiO and High-DiI (c,d) with 0% (red line) and 95% (blue line) DMSO concentration (v/v). The spectra (e), fluorescence photos (f), and DLS results in number % (g) of the High-FRET nanoparticles with 0% (1), 25% (2), 50% (3), 75% (4) and 95% (5) DMSO concentration.

adding DMSO to 95% indicating the dissolution of J-aggregates (Figure 3c,d and Figure S16).

For the High-FRET nanoparticles, we observed a dramatic peak shift from area to area with adding DMSO. To illustrate the disintegration process stepwise, we monitored the whole process by adding DMSO gradually from 25%, 50% to 75% and 95%. At 0% DMSO, the nanoparticle suspension was red in fluorescence color, the FRET peak at area was dominant with a negligible donor peak, demonstrating a high FRET ratio (Figure 3e1,f1). When the DMSO concentration increased to 25%, the suspension changed to orange-red color, the FRET peak at area decreased and increased at area indicating the disruption and loosening of the hybrid FRET cores (Figure 3e2,f2). As the DiO and DiI co-precipitated to form the hybrid FRET-core polymer-shell nanoparticles, the dissolution of the hybrid FRET cores led to the release of DiO and DiI molecules and the diminishing of the hybrid cores. In other words, during the dissolution process, the size of the hybrid FRET nanoparticle cores became smaller and smaller, the amount of DiO and DiI in molecular states increased along with the addition of DMSO. With the increase of DMSO to 50%, the suspension changed to orange and the FRET peak in area completely disappeared, demonstrating all the hybrid FRET cores were dissolved and became dye molecules. As DiO and DiI are both more soluble in DMSO than the polymer, the polymer-shell of the nanoparticles was able to confine some of the dissolved DiO and DiI molecules and keep them in very close proximity, thus leading to the recovery of the FRET emission at area II (Figure 3e3,f3), similar to the Low-FRET nanoparticles at 0% of DMSO. When the DMSO concentration was increased to 75%, the suspension changed to yellow color, the donor peak in area emerged indicating that the polymeric shell started to disassemble resulting in the release and spatial separation of the two dyes (Figure 3e4,f4). Finally, when the DMSO concentration reached 95%, the High-FRET nanoparticles were fully dissolved (no nanoparticle detected by DLS) and the suspension turned to green, only one peak at area showing the full recovery of donor emission with complete separation of the donor and acceptor dyes (Figure 3e5,f5,g5 and Figure S16). For the High-FRET nanoparticles, the FRET ratio III/II decreased from 10.03 to 0.08, the FRET ratio II/I decreased from 119.2 to 0.15 when the DMSO concentration increased from 0% to 95% (Table S4). The DMSO dissolution experiment reveals two release processes of the high dye-loading nanoparticles, that is, the dissolution of dye nano-

particles in the core into dye molecules inside the polymer shell, and the disassembly of the polymer shell leading to the release of dye molecules out of the nanoparticles. This swelling and disassemble process was also demonstrated by monitoring the hydrodynamic size change of the nanoparticles from 126 to 964 nm along with the addition of DMSO (Figure 3 g1–4 and Figure S17). These two individual processes may occur simultaneously or sequentially depending on the dissolution condition, because the dissolution and swelling rates of dyes and polymer are different under different environments. Although the peak shift of the High-DiO or High-DiI nanoparticles during the disintegration is able to provide the information about the dissolution or release of dye molecules, it provides no information about disassembly of polymers. In contrast, monitoring the whole release and disintegration process using High-FRET nanoparticles offers a better understanding of the release and particle disintegration process by closely monitoring the changes of the 3 peaks. Therefore, FRET in combination with J-aggregate induced the red-shift phenomenon, named J-aggregate-based FRET, is ideal to monitor these two individual processes.

Then we evaluated the intracellular drug release kinetics of the Low-FRET and High-FRET nanoparticles using SKOV3 cancer cells (Figure 4). The Low-FRET, High-FRET, and plain polymer nanoparticles were incubated with SKOV3 cells for only 10 min to minimize NP uptake thus better observation of dye release and disassembly kinetics, then free nanoparticles were removed and fresh medium was added. The cells were then incubated further and the spectra of the cell suspension were recorded over time. Cells cultured with plain polymer nanoparticles (without dye) were regarded as the Blank for subtraction.

For the Low-FRET nanoparticles, an increase of the donor peak at area and a decrease of FRET peak at area was observed over time from 0 to 4 h with the FRET ratio II/I decreased from 2.18 to 0.57 (Figure 4 a, Figure S18 and Table S5). The gradually reduced FRET ratio suggested that DiO and DiI molecules were slowly released from the polymeric nanoparticles. The confocal images also show a similar trend (Figure 4 b and Figure S19). At the beginning (0 h), the Low-FRET nanoparticles adhered to the cell membrane as indicated by the bright yellow lines surrounding cells in channel. Then more and more nanoparticles were internalized as reflected by the increasing number of yellow spots inside cells from 0 h to 4 h.[18] The green color from the released DiO started to appear at 0.5 h in channel I and became brighter over time indicating more DiO and DiI molecules were released into the cytoplasm. From 4 h to 12 h, the spectra reached a plateau with a constant FRET ratio (Figure 4 a) and the green color of the channel in the confocal images was much brighter than the yellow color of channel (Figure 4 b and Figure S19). To mimic their stability in lysosomes, we incubated the Low-FRET nanoparticles in artificial lysosomal fluid (ALF) to monitor the size change over 12 h (Table S6). We didn't observe significant size change over the 12 h incubation period, indicating the quick dye release from these low drug-loading nanoparticles was mainly due to drug diffusion (Figure 4 c), which agrees with others' findings.[19]

For the high-FRET nanoparticles, the FRET peak at area was dominating (ON status of red-shift) and the donor peak was negligible (Figure 4 d) at the beginning (0 h). After 0.5 h incubation, the peaks at both area and area increased due to the dissolution of the DiO and DiI molecules in the hybrid FRET cores inside the polymer shell. The donor peak at area emerged as the dissolved dye molecules released from the nanoparticles. This is different from what we observed in the DMSO dissolution experiments, wherein it only shows the increase of peak at area but not area. At 2 h, the FRET peak at area almost disappeared (OFF status of red-shift) with the FRET ratio III/II dropped dramatically from 9.03 to 0.28, the first process terminated with the complete dissolution of the hybrid FRET cores (Figure 4 d, Figure S20 and Table S7).

The confocal images agree with the spectra results (Figure 4 e and Figure S21). Similar to the Low-FRET nanoparticles, the confocal image of High-FRET nanoparticles shows bright red signals at 0 h in channel suggesting strong NP-cell interactions. Then at 0.5 h, yellow signals started to appear in channel II, indicating gradual dissolution of the hybrid FRET cores in the nanoparticles. Also, the cytoplasm of cells was illuminated with green color in channel I, mainly due to the release of DiO and DiI molecules and their spreading in the cells (Figure 4 e and Figure S21). At 2 h, the confocal image confirmed the dramatic decrease of the red color in channel III and the significant increase of the yellow color in channel II, which is consistent with the disappearance of the FRET peak at area III (Figure 4 e and Figure S21).

Afterwards, the second process started with the increase of donor peak at area and a decrease of the FRET peak at area, which was similar to the Low-FRET, and the FRET ratio II/I decreased from 2.08 (at 2 h) to 0.88 (at 8 h) and reached a plateau (Table S7). The spectra reached a plateau with a constant FRET ratio at 8 h and remained stable. For confocal images from 2 h to 8 h, the color of the overlay channel of the confocal image turned from yellow to yellow-green demonstrating the continuous release of DiO and DiI molecules (Figure S21). Even at 12 h, the FRET peak at area was still obvious showing the incomplete recovery of donor emission. The spectra of High-Mixture nanoparticles after incubation with cells for 12 h were similar to the High-FRET nanoparticles as well, suggesting the FRET on the membrane occurred (Figure S22,23). This was similar to what have been observed previously due to the diffusion of the released DiO and DiI molecules to both nucleus and cell membranes.[6c,16] Then the accumulation of both DiO and DiI molecules on membranes within proximity led to the recovery of the FRET ratio to some extent, which compensated the decrease of FRET ratio caused by dye release.

Similarly, we also incubated the High-FRET nanoparticles in the ALF to investigate their size change in lysosomes over 12 h (Table S8). From 0 h to 4 h, the High-FRET nanoparticles illustrated a continuous swelling which had a similar trend as the size change of the High-FRET nanoparticles in DMSO aqueous solution with increasing concentration from 0% to 75% (Figure 3 g1–4). At 8 h, the High-FRET nanoparticles could not be detected which suggested the complete disassembly of the nanoparticles (the same as in the 95% of DMSO), corresponding to the

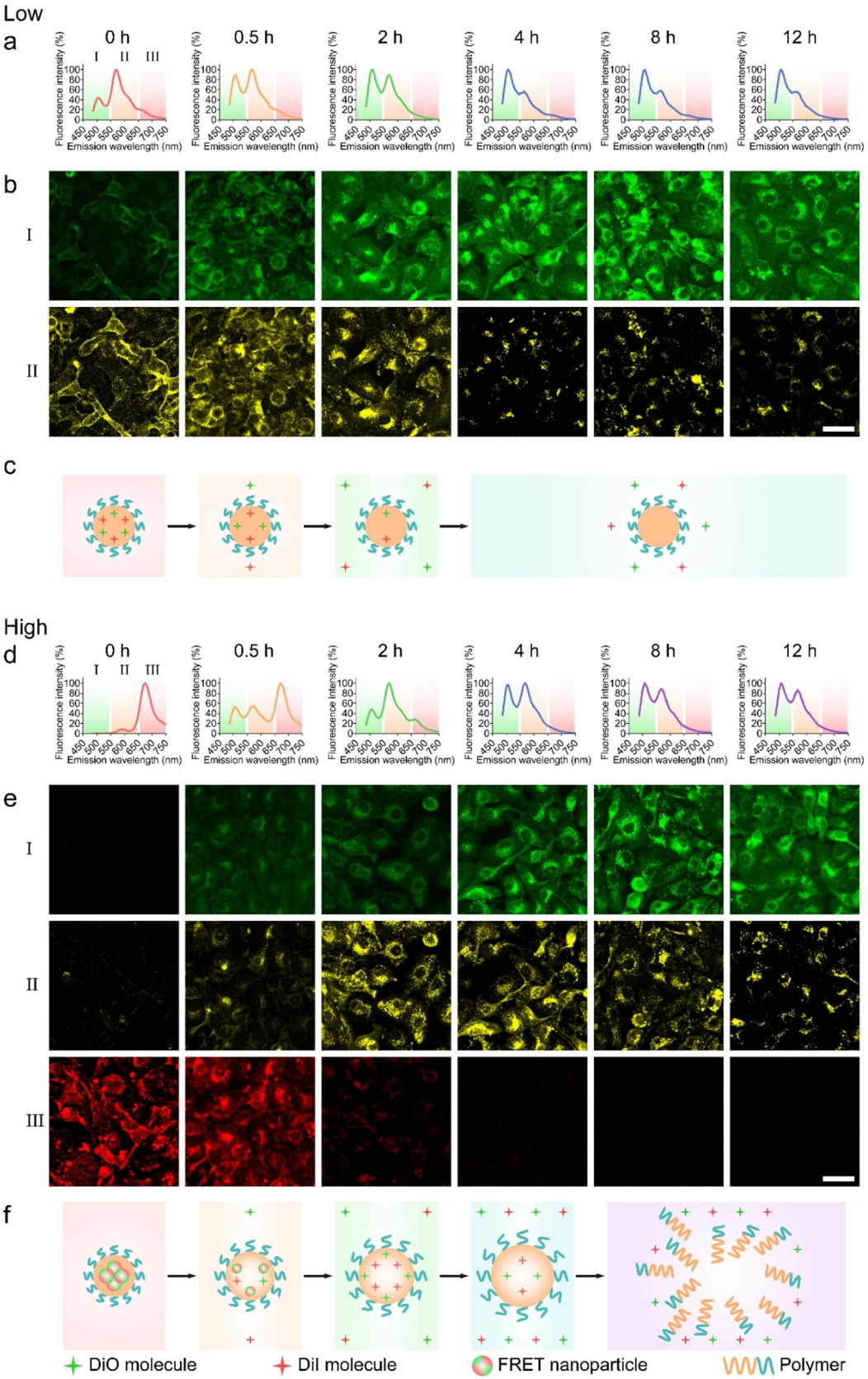

Figure 4. The spectra, confocal images and schemes of dye release and disassembly kinetics of the Low-FRET (a,b,c) and High-FRET (d,e,f) nanoparticles from 0 h to 12 h in SKOV3 cancer cells. Channel information of CLSM: I represents DiO (green, $\lambda_{excitation}$ = 470 nm, $\lambda_{detection}$ = 490–530 nm); II represents Low-FRET (yellow, $\lambda_{excitation}$ = 470 nm, $\lambda_{detection}$ = 550–590 nm); III represents High-FRET (red, $\lambda_{excitation}$ = 470 nm, $\lambda_{detection}$ = 650–690 nm). Scale bar, 50 μm.

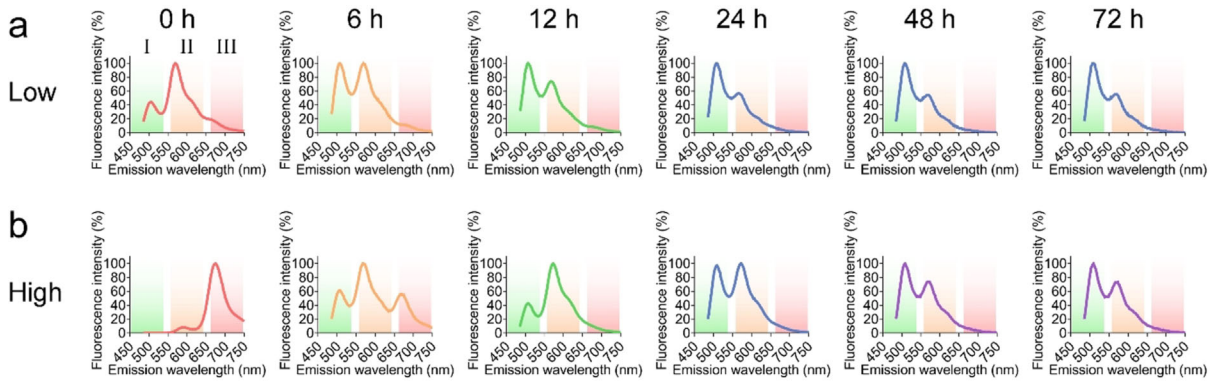

Figure 5. The spectra of release and disassembly kinetics of Low-FRET (a) and High-FRET (b) nanoparticles from 0 h to 72 h in FBS.

plateau of the spectra at 8 h (Figure 4 d). The differences in the size changes between Low-FRET and High-FRET nanoparticles when incubating in ALF implied their different release kinetics. In contrast to the diffusional dye release of the low dye-loading nanoparticles synthesized by the traditional method,[19c] the high dye-loading nanoparticles synthesized by our sequential nanoprecipitation method showed sustained release through dye dissolution, polymer swelling and gradual polymer matrix erosion.[5] This is not surprising because when the drug loading of polymeric nanoparticles with sizes around 100–150 nm increased to 50 wt %, the polymer shell thickness could be only about 10–15 nm. Such a thin layer of polymer with drug nanoparticles dispersed in its matrix, it is easy to swell. To control the polymer swelling thus the drug release, less or no swelling polymers can be used along with PLGA in different ratios. Based on these results, a schematic was proposed (Figure 4 f) showing the release and disassembly processes of the High-FRET nanoparticles. It starts from the dissolution of the hybrid FRET cores into molecular dyes inside the polymer shell from 0 h to 2 h, followed by the release of dye molecules and the swelling of the polymer shell from 0 h to 8 h. The plateau spectra and no detectable nanoparticles in ALF after 8 h indicated the complete disassemble of the nanoparticles.

To compare the release kinetics intracellularly and in serum, we further evaluated the Low-FRET and High-FRET nanoparticles in fetal bovine serum (FBS) for 72 h to mimic their stability during circulation. Overall, the spectra and release processes of the Low-FRET and High-FRET nanoparticles in serum were similar to the intracellular release. For the Low-FRET nanoparticles, the FRET ratio II/I decreased monotonically from 2.25 to 0.57 and reached a plateau at 24 h (Figure 5 a, Figure S24 and Table S9). For the High-FRET nanoparticles, the FRET ratio III/II also decreased monotonically from 9.27 to 0.12, and remained steady from 12 h. The FRET ratio II/I increased from 6 h and peaked at 12 h, then started to drop (Figure 5 b, Figure S25 and Table S10). However, the time required to fully release the dyes in serum was longer for both the Low-FRET (24 h) and High-FRET (48 h) nanoparticles. The degradation of polymeric nanoparticles could be accelerated by acidic pH or/and enzymes, and salt concentration in the environment and temperature also play some roles in controlling their stability and degradation.[20] We conducted a stability study by monitoring the size change of the High-FRET nanoparticles under pH 7.4 and 4.5 at 37 °C with gentle shaking (Table S11), demonstrating that acidic pH did accelerate the disintegration of High-FRET nanoparticles.

Additionally, the intracellular and serum release kinetics as well as the size change of the High-DiO and High-DiI nanoparticles in ALF were compared to those of the High-FRET nanoparticles. The time required for the full dissolution of the dye cores and the complete disassembly of the High-DiO and High-DiI nanoparticles in ALF were similar to that of the High-FRET nanoparticles (Figure S26–33 and Table S12,13). According to the release kinetics of the Low-FRET and High-FRET nanoparticles intracellularly and in serum, the High-FRET nanoparticles showed a slower release kinetic than that of the Low-FRET nanoparticles under both conditions. The release time of the High-FRET nanoparticles was 24 h longer than the Low-FRET nanoparticles in serum indicating improved stability of the High-FRET nanoparticles. However, the release time of the High-FRET nanoparticles was 4 h longer than the Low-FRET nanoparticles in cells. According to our previous in vivo biodistribution experiment,[1b] the polymeric nanoparticles' tumor accumulation started from 2 h after injection and reached the maximum accumulation level at 24 h. Therefore, good stability during circulation is critical, which ensures the efficient delivery of the drug to the targeted locations. For the High-FRET nanoparticles, their longer release time in serum implied their better stability during circulation compared to the Low-FRET nanoparticles. This in-serum stability might explain enhanced therapeutic effect of the high drug-loading nanoparticles in comparison with the low drug-loading nanoparticles in vivo.[5] It has also been reported previously that the increase in drug loading could decrease the drug release rate,[19b] as drug is easier to dissolve in molecular state, but not in particle state. Also, the outer corona region of the polymeric nanoparticles is relatively mobile, drug release from this area is quicker than that from the core area.[19b,21] Therefore, the High-FRET nanoparticles released slower and were more stable than Low-FRET nanoparticles intracellularly and in serum due to the additional process of dissolving drug nanoparticles to drug molecules.

Conclusion

This paper reports for the first time the large red-shift (≈100 nm) in fluorescence spectra with increasing the dye loading (>6.3 wt%) in fluorescent dye-loaded nanoparticles. We investigated the release and disassembly processes of the high drug-loading nanoparticles using a unique J-aggregate-based FRET method. We found that drug release of the drug-core polymer-shell nanoparticles with an exceptionally high drug loading (50 wt%) was slower than the low drug-loading nanoparticles (0.5 wt%) because the high drug-loading nanoparticles have two simultaneous release processes intracellularly and in serum. One is to dissolve the drug core into drug molecules and the other is to release the drug molecules from polymer nanoparticles. Numerous in vitro methods have been developed to monitor drug release from nanoparticles, but most of them have been found very hard or impossible to reveal the intracellular fate of nanoparticles due to the difficulties of accurately distinguishing encapsulated drug and released drug as well as the integrity of nanoparticles especially for nanoparticles with a complex structure such as our high drug-loading nanoparticles. In addition to our spectral results, a detailed photoluminescence lifetime analysis (both in spectroscopy and microscopy) of the various emission peaks with different excitation wavelengths would be interesting to obtain further understanding of the FRET processes at the different stages of nanoparticle disintegration and the differences of Low-FRET and High-FRET nanoparticles. In conclusion, our strategy of using J-aggregate based FRET and the change of spectrum red shift offers a new approach to systematically investigate the structure and release of high drug-loading nanoparticles (>6.3 wt%). It provides a useful tool for screening different nanoparticles with high drug loading, and offers better understanding of their in vitro and in vivo behaviors facilitating the development of promising candidates for further clinical investigation.

Acknowledgements

The project was supported by the Australian Research Council projects (FT140100726 and DP200101238), the National Science Foundation (DMR-1310266), and the Harvard Materials Research Science and Engineering Center (DMR-1420570). The authors acknowledge the facilities, and the scientific and technical assistance, of the Australian Microscopy & Microanalysis Research Facility at the Centre for Microscopy and Microanalysis, The University of Queensland. This work was performed in part at the Queensland node of the Australian National Fabrication Facility. A company established under the National Collaborative Research Infrastructure Strategy to provide nano and microfabrication facilities for Australia's researchers.

Conflict of interest

The authors declare the following competing interests: The University of Queensland (UQ) filed a patent on the core-shell polymer nanoparticles (PCT/AU2019/050557, filed 31 May 2019). Y.L., G.Y. and C.-X.Z. are named inventors on this patent and through their employment with UQ hold an indirect interest in this intellectual property. The other authors declare no competing interest.

Keywords: drug release · FRET · J-aggregates · nanoparticles · polymers

[1] a) R. A. Jain, *Biomaterials* **2000**, *21*, 2475–2490; b) Y. Liu, Y. Hui, R. Ran, G. Z. Yang, D. Wibowo, H. F. Wang, A. P. Middelberg, C. X. Zhao, *Adv. Healthcare Mater.* **2018**, *7*, 1800106; c) A. Pitchaimani, T. D. T. Nguyen, R. Marasini, A. Eliyapura, T. Azizi, M. Jaberi-Douraki, S. Aryal, *Adv. Funct. Mater.* **2019**, *29*, 1806817.

[2] a) H. K. Makadia, S. J. Siegel, *Polymers* **2011**, *3*, 1377–1397; b) D. B. Kaldybekov, S. K. Filippov, A. Radulescu, V. V. Khutoryanskiy, *Eur. J. Pharm. Biopharm.* **2019**, *143*, 24–34.

[3] a) Z. Liu, Y. Jiao, Y. Wang, C. Zhou, Z. Zhang, *Adv. Drug Delivery Rev.* **2008**, *60*, 1650–1662; b) P. Couvreur, *Adv. Drug Delivery Rev.* **2013**, *65*, 21–23; c) G. A. Husseini, W. G. Pitt, *Adv. Drug Delivery Rev.* **2008**, *60*, 1137–1152; d) L. Zhang, J. M. Chan, F. X. Gu, J.-W. Rhee, A. Z. Wang, A. F. Radovic-Moreno, F. Alexis, R. Langer, O. C. Farokhzad, *ACS Nano* **2008**, *2*, 1696–1702; e) Y. Liu, G. Yang, D. Zou, Y. Hui, K. Nigam, A. P. Middelberg, C.-X. Zhao, *Ind. Eng. Chem. Res.* **2020**, *59*, 4134–4149.

[4] G. Yang, Y. Liu, H. Wang, R. Wilson, Y. Hui, L. Yu, D. Wibowo, C. Zhang, A. K. Whittaker, A. P. Middelberg, C.-X. Zhao, *Angew. Chem. Int. Ed.* **2019**, *58*, 14357–14364; *Angew. Chem.* **2019**, *131*, 14495–14502.

[5] Y. Liu, G. Yang, T. Baby, Tengjisi, D. Chen, D. A. Weitz, C.-X. Zhao, *Angew. Chem. Int. Ed.* **2020**, *59*, 4720–4728; *Angew. Chem.* **2020**, *132*, 4750–4758.

[6] a) H. Chen, S. Kim, L. Li, S. Wang, K. Park, J.-X. Cheng, *Proc. Natl. Acad. Sci. USA* **2008**, *105*, 6596–6601; b) T. A. Diezi, Y. Bae, G. S. Kwon, *Mol. Pharm.* **2010**, *7*, 1355–1360; c) J. Lu, S. C. Owen, M. S. Shoichet, *Macromolecules* **2011**, *44*, 6002–6008; d) H. Chen, S. Kim, W. He, H. Wang, P. S. Low, K. Park, J.-X. Cheng, *Langmuir* **2008**, *24*, 5213–5217; e) S. Jiwpanich, J.-H. Ryu, S. Bickerton, S. Thayumanavan, *J. Am. Chem. Soc.* **2010**, *132*, 10683–10685; f) T. Miller, R. Rachel, A. Besheer, S. Uezguen, M. Weigandt, A. Goepferich, *Pharm. Res.* **2012**, *29*, 448–459; g) Z. Dong, Y. Bi, H. Cui, Y. Wang, C. Wang, Y. Li, H. Jin, C. Wang, *ACS Appl. Mater. Interfaces* **2019**, *11*, 23840–23847; h) H. Zhang, H. Li, Z. Cao, J. Du, L. Yan, J. Wang, *J. Controlled Release* **2020**, *324*, 47–54.

[7] a) R. M. Clegg, *Lab. Tech. Biochem. Mol. Biol.* **2009**, *33*, 1–57; b) D. M. Charron, G. Zheng, *Nano Today* **2018**, *18*, 124–136; c) Y. Sun, H. Wallrabe, S. A. Seo, A. Periasamy, *ChemPhysChem* **2011**, *12*, 462–474; d) N.-T. Chen, S.-H. Cheng, C.-P. Liu, J. Souris, C.-T. Chen, C.-Y. Mou, L.-W. Lo, *Int. J. Mol. Sci.* **2012**, *13*, 16598–16623; e) A. Gaudin, O. Tagit, D. Sobot, S. Lepetre-Mouelhi, J. Mougin, T. F. Martens, K. Braeckmans, V. Nicolas, D. Desmaële, S. C. de Smedt, *Chem. Mater.* **2015**, *27*, 3636–3647; f) A. Gaudin, M. Yemisci, H. Eroglu, S. Lepetre-Mouelhi, O. F. Turkoglu, B. Dönmez-Demir, S. Caban, M. F. Sargon, S. Garcia-Argote, G. Pieters, *Nat. Nanotechnol.* **2014**, *9*, 1054–1062.

[8] J. Tao, Z. Wei, Y. He, X. Yan, S. M.-Y. Lee, X. Wang, W. Ge, Y. Zheng, *Biomaterials* **2020**, *256*, 120180.

[9] a) G. W. Gordon, G. Berry, X. H. Liang, B. Levine, B. Herman, *Biophys. J.* **1998**, *74*, 2702 – 2713; b) B. A. Lewis, D. M. Engelman, *J. Mol. Biol.* **1983**, *166*, 211 – 217.
[10] G. S. Kwon, T. Okano, *Adv. Drug Delivery Rev.* **1996**, *21*, 107 – 116.
[11] a) E. E. Jelley, *Nature* **1936**, *138*, 1009 – 1010; b) G. Scheibe, *Angew. Chem.* **1937**, *50*, 212 – 219.
[12] J. L. Bricks, Y. L. Slominskii, I. D. Panas, A. P. Demchenko, *Methods Appl. Fluoresc.* **2017**, *6*, 012001.
[13] F. Würthner, T. E. Kaiser, C. R. Saha-Möller, *Angew. Chem. Int. Ed.* **2011**, *50*, 3376 – 3410; *Angew. Chem.* **2011**, *123*, 3436 – 3473.
[14] F. Y. Han, Y. Liu, V. Kumar, W. Xu, G. Yang, C.-X. Zhao, T. M. Woodruff, A. K. Whittaker, M. T. Smith, *Int. J. Pharm.* **2020**, *581*, 119291.
[15] a) V. N. Kilin, H. Anton, N. Anton, E. Steed, J. Vermot, T. F. Vandamme, Y. Mely, A. S. Klymchenko, *Biomaterials* **2014**, *35*, 4950 – 4957; b) R. Bouchaala, L. Mercier, B. Andreiuk, Y. Mély, T. Vandamme, N. Anton, J. G. Goetz, A. S. Klymchenko, *J. Controlled Release* **2016**, *236*, 57 – 67.
[16] P. Zou, H. Chen, H. J. Paholak, D. Sun, *Mol. Pharm.* **2013**, *10*, 4185 – 4194.
[17] N. Melnychuk, S. Egloff, A. Runser, A. Reisch, A. S. Klymchenko, *Angew. Chem. Int. Ed.* **2020**, *59*, 6811 – 6818; *Angew. Chem.* **2020**, *132*, 6878 – 6885.
[18] L. Kou, Y. D. Bhutia, Q. Yao, Z. He, J. Sun, V. Ganapathy, *Front. Pharmacol.* **2018**, *9*, 27.
[19] a) T. Musumeci, C. Ventura, I. Giannone, B. Ruozi, L. Montenegro, R. Pignatello, G. Puglisi, *Int. J. Pharm.* **2006**, *325*, 172 – 179; b) C. Allen, D. Maysinger, A. Eisenberg, *Colloids Surf. B* **1999**, *16*, 3 – 27; c) N. Kamaly, B. Yameen, J. Wu, O. C. Farokhzad, *Chem. Rev.* **2016**, *116*, 2602 – 2663.
[20] a) Q. Cai, G. Shi, J. Bei, S. Wang, *Biomaterials* **2003**, *24*, 629 – 638; b) Y. Zhang, S. Zale, L. Sawyer, H. Bernstein, *J. Biomed. Mater. Res.* **1997**, *34*, 531 – 538.
[21] M. Yokoyama, S. Fukushima, R. Uehara, K. Okamoto, K. Kataoka, Y. Sakurai, T. Okano, *J. Controlled Release* **1998**, *50*, 79 – 92.

Manuscript received: June 4, 2020
Revised manuscript received: July 29, 2020
Accepted manuscript online: August 2, 2020
Version of record online: ■■ ■■, ■■■■

Research Articles

Nanoparticles

Y. Liu, G. Yang, S. Jin, R. Zhang, P. Chen, L. Wang, D. Chen, D. A. Weitz, C.-X. Zhao* ———— ■■■■–■■■■

J-Aggregate-Based FRET Monitoring of Drug Release from Polymer Nanoparticles with High Drug Loading

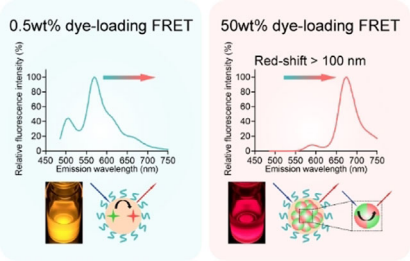

A J-aggregate-based Förster-resonance energy-transfer (FRET) method to investigate the release of high-drug-loading (50 wt%) and low-drug-loading (0.5 wt%) nanoparticles is reported. The high-dye-loading nanoparticles exhibited a slow release kinetics in serum and a relatively quick release in cells, demonstrating their great potential in drug delivery.